BIOCHEMISTRY
including biophysical chemistry & molecular biology
Article

Biochemistry **2009,** *48,* 12125–12132 12125
DOI: 10.1021/bi901439w

Use of 3-Aminotyrosine To Examine the Pathway Dependence of Radical Propagation in *Escherichia coli* Ribonucleotide Reductase[†]

Ellen C. Minnihan,[‡] Mohammad R. Seyedsayamdost,[‡,∥] and JoAnne Stubbe*[,‡,§]

[‡]*Department of Chemistry and* [§]*Department of Biology, Massachusetts Institute of Technology, 77 Massachusetts Avenue, Cambridge, Massachusetts 02139-4307* [∥]*Current address: Department of Biological Chemistry and Molecular Pharmacology, Harvard Medical School, 240 Longwood Ave., C1-609, Boston, MA 02115.*

Received August 16, 2009; Revised Manuscript Received November 13, 2009

ABSTRACT: *Escherichia coli* ribonucleotide reductase (RNR), an $\alpha 2\beta 2$ complex, catalyzes the conversion of nucleoside 5′-diphosphate substrates (S) to 2′-deoxynucleoside 5′-diphosphates. α2 houses the active site for nucleotide reduction and the binding sites for allosteric effectors (E). $\beta 2$ contains the essential diferric tyrosyl radical ($Y_{122}^{\bullet}$) cofactor which, in the presence of S and E, oxidizes C_{439} in α to a thiyl radical, $C_{439}^{\bullet}$, to initiate nucleotide reduction. This oxidation occurs over 35 Å and is proposed to involve a specific pathway: $Y_{122}^{\bullet} \rightarrow W_{48} \rightarrow Y_{356}$ in $\beta 2$ to $Y_{731} \rightarrow Y_{730} \rightarrow C_{439}$ in α2. 3-Aminotyrosine (NH_2Y) has been site-specifically incorporated at residues 730 and 731, and formation of the aminotyrosyl radical ($NH_2Y^{\bullet}$) has been examined by stopped-flow (SF) UV−vis and EPR spectroscopies. To examine the pathway dependence of radical propagation, the double mutant complexes $Y_{356}F$-$\beta 2$:$Y_{731}NH_2Y$-α2, $Y_{356}F$-$\beta 2$:$Y_{730}NH_2Y$-α2, and wt-$\beta 2$:$Y_{731}F/Y_{730}NH_2Y$-α2, in which the nonoxidizable F acts as a pathway block, were studied by SF and EPR spectroscopies. In all cases, no $NH_2Y^{\bullet}$ was detected. To study off-pathway oxidation, Y_{413}, located 5 Å from Y_{730} and Y_{731} but not implicated in long-range oxidation, was examined. Evidence for $NH_2Y_{413}^{\bullet}$ was sought in three complexes: wt-$\beta 2$:$Y_{413}NH_2Y$-α2 (a), wt-$\beta 2$:$Y_{731}F/Y_{413}NH_2Y$-α2 (b), and $Y_{356}F$-$\beta 2$:$Y_{413}NH_2Y$-α2 (c). With (a), $NH_2Y^{\bullet}$ was formed with a rate constant that was 25−30% and an amplitude that was 25% of that observed for its formation at residues 731 and 730. With (b), the rate constant for $NH_2Y^{\bullet}$ formation was 0.2−0.3% of that observed at 731 and 730, and with (c), no $NH_2Y^{\bullet}$ was observed. These studies suggest the evolution of an optimized pathway of conserved Ys in the oxidation of C_{439}.

Long-range electron transfer (ET)[1] (*1*) is prevalent in biology and plays a central role in many processes, including respiration (*2*), nitrogen fixation (*3*), and the photosynthetic reaction centers (*4*). Studies over many decades have established that ET occurs rapidly and efficiently between metal clusters that are spaced 10−15 Å apart (*5*) and that the process involves electron tunneling as described by the Marcus−Levich equation (*6*). The importance of the medium, the intervening polypeptide structural motifs, has been studied extensively in model proteins and biological systems (*1*, *7*). The protein fold clearly plays a central role in lowering the reorganization energy of the biological ET reaction. It is also clear that ET kinetics can be regulated by the dynamics of conformational changes, especially across protein−protein interfaces (*8*, *9*).

The discovery of the central role of a tyrosyl radical ($Y^{\bullet}$) in the class Ia ribonucleotide reductase (*10*) and the O_2-evolving complex of photosystem II (*11*) led to the realization that ET processes over long distances are not limited to metal clusters. Long-range ET can also involve the aromatic amino acids tryptophan and tyrosine, the oxidations of which require loss of both an electron and a proton (*12*). Ribonucleotide reductase (RNR), which catalyzes the conversion of nucleotides to deoxynucleotides (*13*), has served as the paradigm for long-range proton-coupled electron transfer (PCET) with the tyrosyl radical ($Y^{\bullet}$) in the β subunit mediating the oxidation of a cysteine in the α subunit 35 Å away (Figure 1) (*12*, *14*). This paper describes the use of 3-aminotyrosine (NH_2Y), site-specifically incorporated into the α subunit of RNR (*15*), in examining the pathway dependence, and the importance of transient intermediates, proposed for this oxidation.

Tyrosyl radicals ($Y^{\bullet}$) and tryptophan radicals ($W^{\bullet}$) have been studied in three different contexts indirectly related to radical propagation in RNRs. In the area of model proteins and peptides, oxidizable amino acids have been positioned between electron donor:acceptor pairs. Studies of the ET process in the resulting systems have demonstrated rate accelerations associated with a hopping model requiring formation of a transient intermediate (*16*, *17*). These "simple" systems have allowed detailed mechanistic analyses and provide precedent for the multiple hopping steps proposed for RNR.

Y and W radicals have been observed in heme and non-heme iron-dependent proteins, in which a reactive metal-based intermediate generated during catalysis is, in the absence of substrate,

[†]This work was supported by National Institutes of Health Grant GM29595 (to J.S.). E.C.M. was supported by a Koch Graduate Fellowship.

*To whom correspondence should be addressed. Telephone: (617) 253-1814. Fax: (617) 324-0505. E-mail: stubbe@mit.edu.

[1]Abbreviations: α, ribonucleotide reductase large subunit; β, ribonucleotide reductase small subunit; $C^{\bullet}$, thiyl radical; CDP, cytidine 5′-diphosphate; dC, 2′-deoxycytidine; DTT, dithiothreitol; E, effector; EPR, electron paramagnetic resonance; ET, electron transfer; FPLC, fast protein liquid chromatography; $NH_2Y^{\bullet}$, 3-aminotyrosyl radical; PCET, proton-coupled electron transfer; PL, photolyase; RNR, ribonucleotide reductase; S, substrate; SF, stopped-flow; TR, thioredoxin; TRR, thioredoxin reductase; $W^{\bullet}$, tryptophan radical; wt, wild-type; $Y^{\bullet}$, tyrosyl radical.

Published on Web 11/16/2009

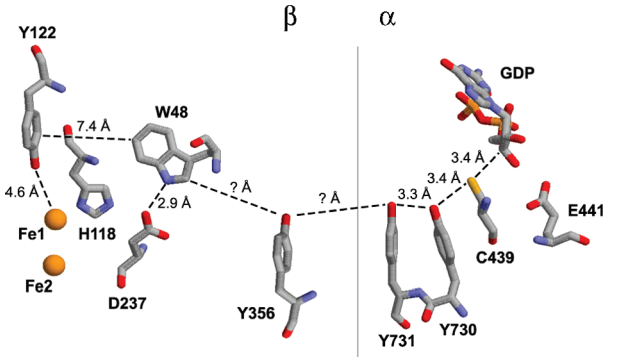

FIGURE 1: Proposed radical propagation pathway within an α:*β* pair of *Escherichia coli* RNR. Y_{356}, Y_{731}, and Y_{730} have been shown to be redox-active during radical transfer, and their positions within the complex have been determined structurally (*14*) and/or experimentally (*35*). Y_{356} is located in the structurally disordered C-terminal tail of *β* (*44*), and thus, its location in the complex is not known.

reduced by ET from an aromatic residue(s) in the vicinity of the metallo cofactor (*18*−*21*). In general, small amounts of multiple radical species are generated on a slow (second) time scale. These systems are starting to define the mechanisms and consequences of aberrant oxidations and provide a model for the phenotype of an off-pathway oxidation in RNR.

Finally, transient aromatic amino acid radicals have been studied in enzymes such as cytochrome *c* peroxidase and prostaglandin synthase, in which metallo cofactors are responsible for the oxidation of aromatic amino acids over short distances in the presence of substrate (*22*, *23*). Only ribonucleotide reductase and photolyase (PL), however, are believed to utilize multiple, transient aromatic amino acid radical intermediates in long-range ET. PL, as isolated, contains a flavin cofactor in the semiquinone form ($FADH^{\bullet}$) that needs to be reduced to its active form ($FADH^{-}$) prior to catalysis (*24*). Time-resolved kinetic studies suggest that the reduction occurs by a hopping mechanism involving three conserved Ws over a 15 Å distance (*25*). To obtain insight into the pathway dependence of reduction of $FADH^{\bullet}$, the nonoxidizable amino acid phenylalanine (F) was incorporated in place of each of the Ws and reanalyzed by ultrafast kinetics (*26*−*28*). The measurements on the wild-type and mutant PLs support a model in which three Ws act as a wire to the flavin cofactor.

The class Ia ribonucleotide reductases are the only known enzymes whose physiological function requires long-range oxidation, thought to occur in a pathway-dependent fashion through a series of aromatic amino acids (Figure 1). This provocative mechanism was first proposed by Uhlin and Eklund on the basis of a docking model of the α2:*β*2 complex and on the basis of the strict conservation of the residues in primary sequence alignments (*14*). Mutagenesis studies in which each of the residues was replaced individually by F demonstrated their importance in catalysis, structure, or both (*29*−*32*). However, only with the advent of technology for the site-specific incorporation of unnatural amino acids into α and *β* has the involvement of the three tyrosines [residue 356 in *β*2 and residues 731 and 730 in α2 (Figure 1)] and the distance of the individual oxidation "steps" been examined (*15*, *33*−*36*). We have demonstrated recently the site-specific incorporation of 3-aminotyrosine (NH_2Y) into the α and *β* subunits at each of these positions. SF UV−vis and EPR studies revealed that $NH_2Y^{\bullet}$ is generated in a nucleotide-dependent manner with multiphasic kinetics, and that the rates of formation are maximized when substrate and effectors are bound (*15*, *37*). In addition, our studies indicated that NH_2Y-αs are capable of supporting nucleotide reduction, suggesting that the observed radical may be an intermediate on the proposed reaction pathway. From these collective studies, we have proposed that radical propagation occurs via orthogonal PCET in the *β*2 subunit, with the proton transferring off-pathway to an amino acid acceptor or to solvent, and via colinear PCET in the α2 subunit, with both the proton and electron transferring between the same donor:acceptor pair (*12*, *15*).

Despite the appeal of a conserved PCET pathway, evidence in support of transient radical intermediates in RNR has been challenging to obtain because the reaction is rate-limited by conformational changes gated by binding of substrates and effectors to α (*38*). In previous efforts to induce light-mediated turnover on a photopeptide:α2 RNR complex, we have observed deoxynucleotide formation and transient formation of a $Y^{\bullet}$ within the peptide, but due to conformational gating, we have thus far been unable to detect transient intermediates within α (*39*, *40*).

NH_2Y is easier to oxidize than Y by 190 mV at pH 7 (*15*). From a thermodynamic perspective, the detection of $NH_2Y^{\bullet}$ in NH_2Y-αs may not be entirely surprising. Thus, the pathway dependence of $NH_2Y^{\bullet}$ formation is important to establish (Figure 1). To provide further support for a defined pathway, F has been incorporated in place of each Y in the pathway to function as a block of $NH_2Y^{\bullet}$ formation. Incubation of the $Y_{356}F$-*β*2:$Y_{731}NH_2Y$-α2, $Y_{356}F$-*β*2:$Y_{730}NH_2Y$-α2, or wt-*β*2:$Y_{731}F/Y_{730}NH_2Y$-α2 with CDP and ATP completely blocks NH_2Y oxidation, supporting the importance of a specific pathway. As a further test of the pathway dependence, residue Y_{413} was selected for site-specific "off-pathway" NH_2Y incorporation because of its proximity to Y_{731} and Y_{730} in α. Analogous studies were conducted with wt-*β*2:$Y_{413}NH_2Y$-α2, wt-*β*2:$Y_{731}F/Y_{413}NH_2Y$-α2, and $Y_{356}F$-*β*2:$Y_{413}NH_2Y$-α2 complexes in which evidence of $NH_2Y^{\bullet}$ formation was sought by SF and EPR spectroscopy. The results of these experiments establish that functional long-range PCET in RNR occurs via an optimized pathway of amino acids spanning >35 Å across the α:*β* interface.

MATERIALS AND METHODS

Materials. The expression and purification of wt-α2 (2500 nmol min^{-1} mg^{-1}), wt-*β*2 (1.2 $Y_{122}^{\bullet}$/dimer, 7600 nmol min^{-1} mg^{-1}), $Y_{731}NH_2Y$-α2 (150 nmol min^{-1} mg^{-1}), $Y_{730}NH_2Y$-α2 (110 nmol min^{-1} mg^{-1}), His-$Y_{356}F$-*β*2 (1.0−1.2 $Y_{122}^{\bullet}$/dimer, <1 nmol min^{-1} mg^{-1}), and $Y_{730}F$-α2 (<25 nmol min^{-1} mg^{-1}) were conducted as previously described (*15*, *38*, *41*). His-$Y_{356}F$-*β*2 will be termed "$Y_{356}F$-*β*2" henceforth. *E. coli* thioredoxin (TR, 40 units/mg) and thioredoxin reductase (TRR, 1400 units/mg) were isolated as previously described (*41*). [5-^{3}H]CDP was purchased from ViTrax (Placentia, CA).

Generation of pTrc-nrdA-TAG$_{730}$TTT$_{731}$, pTrc-nrdA-TAG$_{413}$, and pTrc-nrdA-TAG$_{413}$TTT$_{731}$. The QuikChange kit (Stratagene) was used according to the manufacturer's instructions to generate pTrc-*nrdA*-$TAG_{730}TTT_{731}$, pTrc-*nrdA*-TAG_{413}, and pTrc-*nrdA*-$TAG_{413}TTT_{731}$. To generate pTrc-*nrdA*-$TAG_{730}TTT_{731}$, the template, pTrc-*nrdA*-TAG_{730} (*15*), was amplified in the presence of forward (5′-TTC GGG GTC AAA ACA CTG TAG TTT CAG AAC ACC CGT GAC GGC GCT-3′) and reverse (5′-AGC GCC GTC ACG GGT GTT CTG AAA CTA CAG TGT TTT GAC CCC GAA-3′) primers to

insert a TTT codon (Phe) at residue 731. To generate pTrc-*nrdA*-TAG_{413}, the template, pTrc-*nrdA*-wt, was amplified in the presence of forward (5′-GCG TCT ACC GGT CGT ATC TAG ATT CAG AAC GTT GAC CAC TGC-3′) and reverse (5′-GCA GTG GTC AAC GTT CTG AAT CTA GAT ACG ACC GGT AGA CGC-3′) primers to insert the amber stop codon (TAG) at residue 413. pTrc-*nrdA*-$TAG_{413}TTT_{731}$ was then generated from pTrc-*nrdA*-TAG_{413}, with forward (5′-C GGG GTC AAA ACA CTG TAT TTT CAG AAC ACC CGT GAC G-3′) and reverse (5′-C GTC ACG GGT GTT CTG AAA ATA CAG TGT TTT GAC CCC G-3′) primers to insert a TTT codon (Phe) at residue 731. For each plasmid, the mutation(s) was confirmed by sequencing the entire gene at the MIT Biopolymers Laboratory.

Expression, Purification, and Determination of the Activity of $Y_{731}F/Y_{730}NH_2Y$-α2. $Y_{731}F/Y_{730}NH_2Y$-α2 was expressed, purified, and prereduced as described for $Y_{730}NH_2Y$-α2 and $Y_{731}NH_2Y$-α2 (*15*). The specific activity was determined by the radioactive RNR assay (*33*). Assays were conducted with mutant α2 and wt-β2 at concentrations of 0.5 and 2.5 μM, respectively, in 50 mM HEPES, 15 mM $MgSO_4$, and 1 mM EDTA (pH 7.6) (assay buffer) at 25 °C. [5-^{3}H]CDP had a specific activity of 1450 cpm/nmol. The reaction product was dephosphorylated by treatment with alkaline phosphatase, and the resulting dC was quantitated by the method of Steeper and Steuart (*33*).

Expression, Purification, and Determination of the Activity of $Y_{413}NH_2Y$-α2 and $Y_{731}F/Y_{413}NH_2Y$-α2. $Y_{413}NH_2Y$-α2 and $Y_{731}F/Y_{413}NH_2Y$-α2 were expressed and purified as described for $Y_{730}NH_2Y$-α2 and $Y_{731}NH_2Y$-α2 (*15*). However, an additional step using a Poros HQ/20 FPLC anion exchange column (Applied Biosystems, 1.6 cm × 10 cm, 20 mL) was required to produce a protein of >95% purity as judged by SDS−PAGE analysis. The column was equilibrated in 50 mM Tris, 1 mM EDTA, and 5 mM DTT (pH 7.6) and was loaded with 15−20 mg of $Y_{413}NH_2Y$-α2 or $Y_{731}F/Y_{730}NH_2Y$-α2. The column was washed with 1 column volume of equilibration buffer at a flow rate of 4 mL/min and then eluted with a linear gradient from 100 to 500 mM NaCl (60 mL × 60 mL) in the same buffer at the same flow rate. In the case of $Y_{731}F/Y_{730}NH_2Y$-α2, the protein was chromatographed twice. Subsequent to the FPLC purification step, the protein was prereduced according to the standard procedure (*15*).

The activities of $Y_{413}NH_2Y$-α2 and $Y_{731}F/Y_{413}NH_2Y$-α2 were determined using the spectrophotometric (*41*) and/or radioactive assays (*33*), with minor modifications. Mutant α2s (0.1 or 0.2 μM) were assayed in the presence of a 5-fold excess of β2 (0.5 or 1.0 μM) in assay buffer at 25 °C. [5-^{3}H]CDP had activity between 2700 and 4800 cpm/nmol.

Determination of the K_d for $Y_{413}NH_2Y$-α2 and β2 Interaction. The K_d between $Y_{413}NH_2Y$-α2 and wt-β2 was determined using $Y_{730}F$-α2 as a competitive inhibitor of nucleotide reduction (*29*, *42*). $Y_{413}NH_2Y$-α2 (0.7 μM) and β2 (0.35 μM) were incubated with CDP (1 mM), ATP (1.6 mM), TR (50 μM), TRR (1 μM), and NADPH (0.2 mM) in assay buffer. Inhibition of RNR activity (as measured by the decrease in NADPH consumption) was determined in the presence of an increasing concentration of $Y_{730}F$-α2 (from 0.1 to 3 μM). The data analysis for this procedure typically relies on the mutant α2 of unknown K_d acting as the inhibitor of nucleotide reduction (*36*). The analysis was modified, as the K_d of the active $Y_{413}NH_2Y$-α2 is not known, whereas the K_d of the inhibitor ($Y_{730}F$-α2) had been previously determined under conditions in which the K_i and K_d of the inhibitor are equivalent (*30*). The K_d for the $Y_{413}NH_2Y$-α2:wt-β2 complex was approximated, and the experimentally determined relative activities were then used to extrapolate the K_d for the $Y_{730}F$-α2:wt-β2 complex. The K_d for $Y_{413}NH_2Y$-α2 was refined by iterative fitting of the experimental data until the fit yielded a K_d for $Y_{730}F$-α2 that was in good agreement with the literature value.

Reaction of NH_2Y-α2s with $Y_{356}F$-β2 Monitored by EPR Spectroscopy. Prereduced $Y_{730}NH_2Y$-α2 or $Y_{731}NH_2Y$-α2 (final concentration of 15 μM) was mixed with $Y_{356}F$-β2 (15 μM, 1 $Y^{\bullet}$/β2) , CDP (1 mM), and ATP (3 mM) in assay buffer at 25 °C. The reactions were quenched at 20 s or 2 min by hand in liquid N_2. The reaction of $Y_{413}NH_2Y$-α2 and $Y_{356}F$-β2 was conducted similarly, except the final protein concentration was 50 μM. EPR spectra were recorded at 77 K on a Brüker ESP-300 X-band spectrometer equipped with a quartz finger dewar containing liquid N_2 in the Department of Chemistry Instrumentation Facility. EPR parameters were as follows: microwave frequency, 9.34 GHz; power, 30 μW; modulation amplitude, 1.5 G; modulation frequency, 100 kHz; time constant, 5.12 ms; scan time, 41.9 s. EPR spin quantitation was conducted in WinEPR (Brüker) using Cu^{II} as a standard (*43*). EPR subtractions were conducted with an in-house, Excel-based program using the spectrum of $Y_{122}^{\bullet}$ from either wt β2 or a wt-β2:mutant-α2 complex as a reference.

Reaction of NH_2Y-α2s with $Y_{356}F$-β2 Monitored by SF UV−Vis Spectroscopy. SF kinetics were determined on an Applied Photophysics DX 17MV instrument equipped with the Pro-Data upgrade. Prereduced $Y_{730}NH_2Y$-α2 (or $Y_{731}NH_2Y$-α2) and ATP were mixed with $Y_{356}F$-β2 and CDP to yield final concentrations of 8 μM, 3 mM, 8 μM, and 1 mM, respectively, in assay buffer at 25 °C. The concentrations of $Y_{122}^{\bullet}$, $NH_2Y_{731}^{\bullet}$, and $NH_2Y_{730}^{\bullet}$ were monitored at 410 nm (ε = 3700 M^{-1} cm^{-1}), 320 nm (ε = 11000 M^{-1} cm^{-1}), and 325 nm (ε = 10500 M^{-1} cm^{-1}), respectively, using PMT detection. In each experiment, five to seven traces were averaged and kinetic parameters obtained by curve fitting using OriginPro or Kaleidagraph. Iterative rounds of fitting were conducted until both the residual plot and the r^2 correlation value were optimized.

Reaction of $Y_{731}F/Y_{730}NH_2Y$-α2, $Y_{413}NH_2Y$-α2, and $Y_{731}F/Y_{413}NH_2Y$-α2 with wt-β2 Monitored by EPR and SF UV−Vis Spectroscopies. $Y_{731}F/Y_{730}NH_2Y$-α2, $Y_{413}NH_2Y$-α2, or $Y_{731}F/Y_{413}NH_2Y$-α2 was reacted with wt-β2 in the presence of CDP and ATP at 25 °C as described for NH_2Y-α2s above. For the EPR and SF experiments, the concentrations of α2 and β2 were 50 and 5 μM, respectively. The EPR reactions were hand quenched at 40 s. The EPR spectrum of putative $NH_2Y_{413}^{\bullet}$ was obtained subsequent to subtraction of the spectrum of $Y_{122}^{\bullet}$ (in the wt-β2:mutant α2 complex) as described above.

RESULTS

Reaction of $Y_{730}NH_2Y$-α2 (or $Y_{731}NH_2Y$-α2) with $Y_{356}F$-β2 Monitored by EPR and SF Spectroscopies. It was previously demonstrated that reaction of either $Y_{730}NH_2Y$-α2 or $Y_{731}NH_2Y$-α2 with wt-β2, CDP, and ATP resulted in the loss of $Y_{122}^{\bullet}$ (λ_{max} = 410 nm; g_{av} = 2.0047) concomitant with formation of a new radical species, assigned as $NH_2Y^{\bullet}$ on the basis of its absorbance and EPR spectroscopic features (λ_{max} = 320−325 nm; g_{av} of 2.0043) (*15*). In this paper, experiments with $Y_{356}F$-β2, in which the radical propagation pathway is disrupted

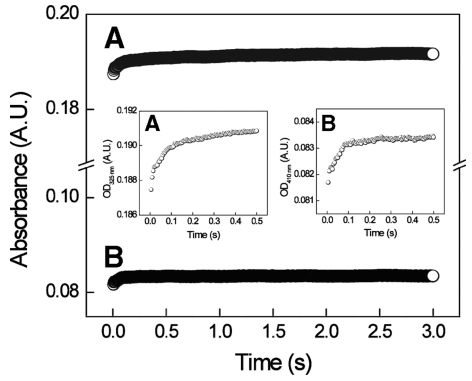

FIGURE 2: SF UV−vis spectroscopy of the reaction of $Y_{356}F$-β2 with $Y_{730}NH_2Y$-α2 in the presence of CDP and ATP. The reaction was monitored at 325 nm (trace A, λ_{max} of $NH_2Y_{730}^{\bullet}$) and at 410 nm (trace B, λ_{max} of $Y_{122}^{\bullet}$). Insets show magnified views of the initial 0.5 s of each trace.

with a Y to F mutation, were conducted to establish that trapping of $NH_2Y^{\bullet}$ at residues 730 and 731 is the result of the participation of these residues in radical transfer, rather than the consequence of introduction of a pathway-independent thermodynamic trap into α2. If formation of $NH_2Y_{730}^{\bullet}$ or $NH_2Y_{731}^{\bullet}$ requires a redox-active Y_{356} residue, then no $NH_2Y^{\bullet}$ should be observed. Reactions were conducted with CDP, ATP, $Y_{356}F$-β2, and $Y_{730}NH_2Y$-α2 (or $Y_{731}NH_2Y$-α2) and quenched at 77 K after 20 s and 2 min. Analysis of the EPR spectra, subsequent to subtraction of the spectrum of resting $Y_{122}^{\bullet}$ at time zero, gave no evidence of $NH_2Y^{\bullet}$ at either time point for reactions with $Y_{730}NH_2Y$-α2 or $Y_{731}NH_2Y$-α2 (Figure S1 of the Supporting Information). In addition, spin quantitation of the signal at time zero in comparison to times 20 s and 2 min revealed no significant loss of spin. A control with nontagged $Y_{356}F$-β2 gave the same result that was observed with His-$Y_{356}F$-β2, demonstrating that the His tag does not interfere with radical formation. Oxidation of Y_{356} is thus a prerequisite for hole migration into the α2 subunit.

To determine if $NH_2Y^{\bullet}$ was formed transiently, the reactions of NH_2Y-α2s with $Y_{356}F$-β2, CDP, and ATP were monitored by SF UV−vis spectroscopy at 325 nm (λ_{max} of $NH_2Y_{730}^{\bullet}$) or 320 nm (λ_{max} of $NH_2Y_{731}^{\bullet}$) and at 410 nm (λ_{max} of $Y_{122}^{\bullet}$). The results for $Y_{730}NH_2Y$-α2 with $Y_{356}F$-β2 are shown in Figure 2 and for $Y_{731}NH_2Y$-α2 with $Y_{356}F$-β2 in Figure S2 of the Supporting Information. A small increase at 325 nm (320 nm) corresponding to ~2% of total initial $Y_{122}^{\bullet}$ was observed. However, these spectral changes were not correlated with the expected decrease in absorbance at 410 nm due to loss of the $Y^{\bullet}$. In fact, a small increase in this wavelength was observed (Figure 2 and Figure S2 of the Supporting Information, inset). The lack of correspondence between the spectral changes at 325 nm (or 320 nm) and 410 nm indicates these features are not related to $NH_2Y^{\bullet}$ formation. The nature of these changes is not understood at present, but similar changes have been observed previously under different reaction conditions (*37*) and may be related to minor structural changes of the $Y_{122}^{\bullet}$ diferric cluster upon formation of the α2:β2 complex (M. R. Seyedsayamdost, E. C. Minnihan, and J. Stubbe, unpublished results). The SF UV−vis and EPR spectroscopic data together indicate that no $NH_2Y^{\bullet}$ is formed at residue 730 or 731 with $Y_{356}F$-β2, with our lower limit of detection approximated to be <2% (by SF UV−vis) and <3% (by EPR) of the total initial $Y_{122}^{\bullet}$. These data support the conclusion that a redox-active residue at position 356 is essential for the transfer of radical into α2.

FIGURE 3: Location of Y_{413} (magenta) in relation to Y_{731} (blue), Y_{730} (blue), and C_{439} (yellow) of the radical propagation pathway within the α subunit. Y_{413} is 5.0 and 5.2 Å from Y_{730} and Y_{731}, respectively, with distances measured between phenolic oxygens (red). This figure was generated as a PyMol (www.pymol.org) rendition of Protein Data Bank entry 1RLR (*14*).

Reaction of $Y_{731}F/Y_{730}NH_2Y$-α2 with wt-β2 Monitored by EPR and SF Spectroscopies. To assess the role of residue Y_{731} in the radical transfer chain, the double mutant $Y_{731}F/Y_{730}NH_2Y$-α2 was isolated, characterized, and examined for $NH_2Y^{\bullet}$ formation. The protein was purified to homogeneity and its specific activity measured to be 36 nmol min^{-1} mg^{-1}. This low activity, approximately 1.4% of that of the wild-type enzyme, is likely associated with copurification of endogenous α2, rather than activity inherent to the mutant protein. This result is in agreement with the activity of $Y_{731}F$-α2 (26 nmol min^{-1} mg^{-1}) and contrasts with activities measured in $Y_{730}NH_2Y$-α2 or $Y_{731}NH_2Y$-α2 (110−150 nmol min^{-1} mg^{-1}) (*15*).

$Y_{731}F/Y_{730}NH_2Y$-α2 and ATP were mixed with wt-β2 and CDP, and the reaction was examined by EPR and SF spectroscopy. With EPR, the reactions were quenched at 40 s or 2 min and analyzed as described above. No $NH_2Y^{\bullet}$ formation was detected in either case, and the total spin relative to starting $Y_{122}^{\bullet}$ remained unchanged (Figure S3 of the Supporting Information). The SF UV−vis experiments gave results similar to those observed with $Y_{356}F$-β2 at both 325 and 410 nm (Figure S3 of the Supporting Information). Thus, formation of $NH_2Y_{730}^{\bullet}$ also requires a redox-active Y_{731} for radical propagation.

Expression, Purification, and Characterization of $Y_{413}NH_2Y$-α2 and $Y_{731}F/Y_{413}NH_2Y$-α2. As an additional test of the pathway dependence of $NH_2Y^{\bullet}$ formation at Y_{730} and Y_{731}, NH_2Y was site-specifically incorporated at a Y in α2 that is thought not to participate in the radical transfer pathway (Figure 1). Residue Y_{413} was selected, as the X-ray structure of *E. coli* α2 (*14*) reveals distances of 5.0 or 5.2 Å between the phenolic oxygen of Y_{413} and that of Y_{730} or Y_{731}, respectively (Figure 3). Thus, Y_{413} is a distance from Y_{730} and Y_{731} that is reasonable for ET between these residues. Y_{731} and Y_{730} are separated by 3.3 Å in the same structure. Alignment of 142 primary sequences of class Ia/b α2s reveals that while residue 413 is not conserved, it is always an aromatic amino acid. Y, F, and W occupy this position 65, 21, and 14% of the time, respectively. Thus, proteins $Y_{413}NH_2Y$-α2 and $Y_{731}F/Y_{413}NH_2Y$-α2 were

expressed and purified so they could be examined for $NH_2Y^{\bullet}$ formation.

$Y_{413}NH_2Y$-α2 and $Y_{731}F/Y_{413}NH_2Y$-α2 were expressed in a fashion analogous to other NH_2Y-substituted α2s. Their purification, however, proved to be more difficult than for previous NH_2Y-substituted α2s. High-purity protein (as judged by SDS−PAGE) was eventually isolated via anion-exchange FPLC with an optimized salt gradient, but at the expense of overall protein yield (Figure S4 of the Supporting Information).

The activities of the purified mutants were determined by the spectrophotometric and/or radioactive RNR assays. The specific activity of $Y_{413}NH_2Y$-α2 was 46% of that of wt-α2 (~1200 nmol min^{-1} mg^{-1}), while that of $Y_{731}F/Y_{413}NH_2Y$-α2 was 1.9% of that of wt-α2 (~48 nmol min^{-1} mg^{-1}). The activity of $Y_{731}F/Y_{413}NH_2Y$-α2 is similar to that of $Y_{731}F/Y_{730}NH_2Y$-α2 and is likely associated with endogenous *E. coli* α2 that copurified with the recombinantly expressed mutant protein.

The reduction in activity of $Y_{413}NH_2Y$-α2 relative to that of wt-α2, the proximity of Y_{413} to the putative α2:β2 interface, and the difficulty encountered in purification of the related mutants provided the impetus to determine the K_d for the interaction between this mutant and β2 using a modified version of the competitive inhibition assay developed by Climent et al. (*29*, *36*, *42*). Data analysis was modified relative to the previously published method (*36*) because the active species, rather than the inhibitor, was also the species with the unknown K_d (Figure S5 of the Supporting Information). Analysis by this method afforded a K_d of 0.05 μM, similar to the value of 0.06 μM for the wt-α2:β2 complex in the presence of CDP and ATP (A. Q. Hassan and J. Stubbe, unpublished results). This finding, in conjunction with the activity of $Y_{413}NH_2Y$-α2, suggests that $Y_{413}NH_2Y$-α2 is folded and that binding between subunits is minimally perturbed. However, attempts to crystallize $Y_{413}NH_2Y$-α2 under conditions optimized for wt-α2 and successfully used to crystallize other NH_2Y-α2 mutants failed to provide crystals of $Y_{413}NH_2Y$-α2, suggesting that mutation of Y_{413} produces some effect on protein stability or solubility (U. Uhlin and J. Stubbe, unpublished results).

Reactions of $Y_{413}NH_2Y$-α2 or $Y_{731}F/Y_{413}NH_2Y$-α2 with wt-β2 and $Y_{413}NH_2Y$-α2 with $Y_{356}F$-β2 Monitored by EPR Spectroscopy. EPR experiments were conducted as described above by mixing $Y_{413}NH_2Y$-α2 (or $Y_{731}F/Y_{413}NH_2Y$-α2) with CDP, ATP, and wt-β2 or $Y_{413}NH_2Y$-α2 with CDP, ATP, and $Y_{356}F$-β2. Each reaction was quenched at 40 s. The resulting spectra, subsequent to subtraction of the $Y_{122}^{\bullet}$ in the mutant α2:β2 complex, are shown in Figure 4, and the spin quantitation of the resulting $NH_2Y^{\bullet}$ is given in Table 1. In the reactions of $Y_{413}NH_2Y$-α2 and $Y_{731}F/Y_{413}NH_2Y$-α2 with wt-β2 (panels A and B of Figure 4, respectively), the difference EPR spectrum reveals features characteristic of an $NH_2Y^{\bullet}$. For the reaction with $Y_{413}NH_2Y$-α2, the signal attributed to $NH_2Y^{\bullet}$ accounts for 12% of the total spin. Differences in the spectral features relative to those previously reported for $NH_2Y_{730}^{\bullet}$ and $NH_2Y_{731}^{\bullet}$ cannot be assigned at this stage but perhaps report on differences in the dihedral angles of the C_β protons on NH_2Y at position 413 versus those at positions 730 and 731. For the reaction with $Y_{731}F/Y_{413}NH_2Y$-α2, the signal attributed to $NH_2Y^{\bullet}$ accounts for 7% of the total spin. The magnitude of the signal in both cases is substantially lower than that of the "on-pathway" radicals, which have been shown by EPR to constitute 53 or 45% of the total spin at the same time point when NH_2Y is

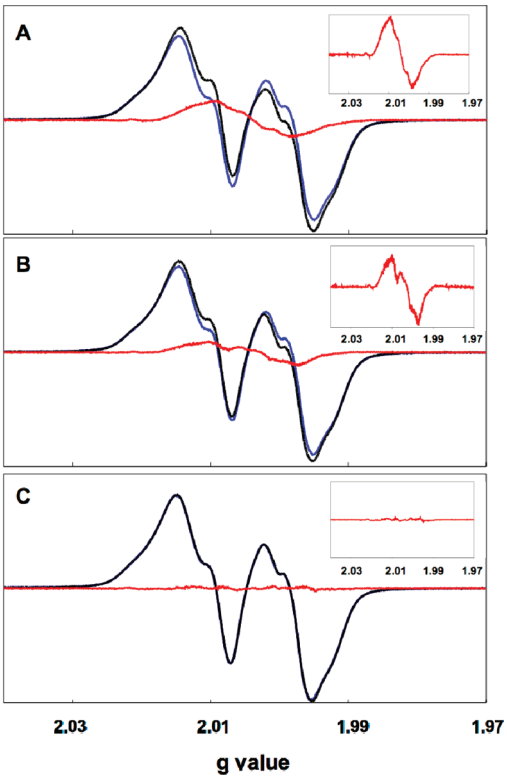

FIGURE 4: Formation of $NH_2Y_{413}^{\bullet}$ monitored by EPR spectroscopy. In each case, CDP and ATP were mixed at 25 °C with (A) wt-β2 and $Y_{413}NH_2Y$-α2, (B) wt-β2 and $Y_{731}F/Y_{413}NH_2Y$-α2, and (C) $Y_{356}F$-β2 and $Y_{413}NH_2Y$-α2, and the reactions were quenched at 77 K after 40 s. For each reaction, the residual $Y_{122}^{\bullet}$ signal (blue) was subtracted from the composite reaction spectrum (black) to give a putative $NH_2Y_{413}^{\bullet}$ (red). The inset gives an expanded view of the difference spectrum, which in the case of panels A and B corresponds to the putative $NH_2Y_{413}^{\bullet}$.

incorporated at position 730 or 731, respectively (*15*). The difference EPR spectrum from the reaction of $Y_{413}NH_2Y$-α2 with $Y_{356}F$-β2, CDP, and ATP quenched at 40 s reveals no detectable $NH_2Y^{\bullet}$ (Figure 4C).

Reaction of $Y_{413}NH_2Y$-α2 or $Y_{731}F/Y_{413}NH_2Y$-α2 with wt-β2 Monitored by SF UV−Vis Spectroscopy. Given the results of the EPR experiments described above, the kinetics of formation of $NH_2Y_{413}^{\bullet}$ were assessed for both $Y_{413}NH_2Y$-α2 and $Y_{731}F/Y_{413}NH_2Y$-α2 using SF UV−vis spectroscopy. The results with $Y_{413}NH_2Y$-α2 and $Y_{731}F/Y_{413}NH_2Y$-α2 are shown in panels A and B of Figure 5, respectively, and are summarized in Table 1. For the reaction with $Y_{413}NH_2Y$-α2 monitored at 325 nm, the observed absorbance increase may be fit to biphasic kinetics with rate constants of 26.4 and 4.2 s^{-1}. These phases correspond to 30 and 70%, respectively, of the total absorbance increase observed at 325 nm over the reaction course. The faster phase is not correlated, however, with a decrease at 410 nm and thus is not associated with $NH_2Y^{\bullet}$ formation.

The A_{410} decrease can be fit to biphasic kinetics with rate constants of 5.3 and 0.5 s^{-1}, corresponding to 47 and 53% of the total absorbance change, respectively, at 410 nm during the reaction. The rate constant of 5.3 s^{-1} agrees well with the rate constant of 4.2 s^{-1} at 325 nm, and together, they suggest the formation of $NH_2Y_{413}^{\bullet}$. Using the extinction coefficients of $NH_2Y^{\bullet}$ and $Y^{\bullet}$, the extent of formation of $NH_2Y_{413}^{\bullet}$ was determined to be 8% of that of the starting $Y_{122}^{\bullet}$. This is substantially lower than the amount of $NH_2Y^{\bullet}$ observed in SF UV−vis studies with NH_2Y at positions 730 (39%) and 731

Table 1: Characterization of $NH_2Y^\bullet$ Formation in α:β Complexes with Various On- and Off-Pathway Mutations

β:α complex	% $NH_2Y^\bullet$ (EPR)[a]	% $NH_2Y^\bullet$ (SF UV−vis)[a]	first-phase k_{obs} (s^{-1})	second-phase k_{obs} (s^{-1})
wt-β2:$Y_{730}NH_2Y$-α2[b]	53	39	12.8	2.5
wt-β2:$Y_{731}NH_2Y$-α2[b]	45	35	19.2	2.7
$Y_{356}F$-β2:$Y_{730}NH_2Y$-α2	< 3[c]	< 2[c]	−	−
$Y_{356}F$-β2:$Y_{731}NH_2Y$-α2	< 3	< 2	−	−
wt-β2:$Y_{731}F/Y_{730}NH_2Y$-α2	< 3	< 2	−	−
wt-β2:$Y_{413}NH_2Y$-α2	12	8	4.8[d]	0.5
wt-β2:$Y_{731}F/Y_{413}NH_2Y$-α2	7	12	0.04	−
$Y_{356}F$-β2:$Y_{413}NH_2Y$-α2	< 3	ND[e]	−	−

[a] $Y_{122}^\bullet$ converted to $NH_2Y^\bullet$, as a percent of the starting $Y_{122}^\bullet$ concentration. [b] Originally reported in ref *15*. [c] No conversion detected within our lower limit of detection, approximated to be 3% of the total initial $Y_{122}^\bullet$ by EPR and 2% by SF UV−vis spectroscopy. [d] Taken as the average of the rate constants measured at 325 and 410 nm. [e] Not determined.

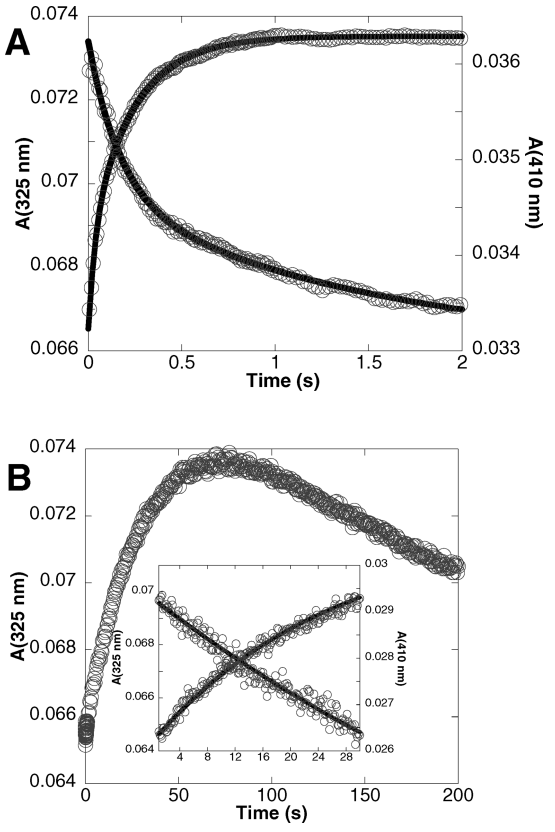

FIGURE 5: Reaction of wt-β2, CDP, ATP, and (A) $Y_{413}NH_2Y$-α2 or (B) $Y_{731}F/Y_{413}NH_2Y$-α2 monitored by SF UV−vis spectroscopy. The reaction was monitored for an increase at 325 nm (λ_{max} of $NH_2Y_{413}^\bullet$) and a decrease at 410 nm (λ_{max} of $Y_{122}^\bullet$). The reaction with $Y_{413}NH_2Y$-α2 (A) was complete within 2 s. The reaction with $Y_{731}F/Y_{413}NH_2Y$-α2 was monitored over 200 s (B), with the first 30 s expanded in the inset. Exponential fits to the data are indicated by solid black lines.

(35%) under analogous reaction conditions (*15*). While a rate constant of 4−5 s^{-1} is fast enough to be involved in production of dNDPs, the collective data on the three Y_{413} mutant complexes suggest $NH_2Y_{413}^\bullet$ formation is off-pathway, and we propose that it is not functionally relevant to catalysis.

For the reaction of $Y_{731}F/Y_{413}NH_2Y$-α2, a slow increase in A_{325} was observed concomitant with a loss of absorbance at 410 nm (Figure 5B). The first 30 s of data collected at both wavelengths were fit to a monoexponential function with a rate constant of 0.04 s^{-1}. The SF data suggest that 12% of the starting $Y_{122}^\bullet$ is converted to $NH_2Y_{413}^\bullet$ over the course of 30 s. The slow rate of radical formation, 320−475-fold slower than the rate of $NH_2Y^\bullet$ formation at position 730 (13 s^{-1}) or 731 (19 s^{-1}), suggests off-pathway oxidation.

DISCUSSION

The rate and extent of $NH_2Y^\bullet$ formation in the presence of the β subunit and the S:E CDP:ATP pair (when NH_2Y has been site-specifically incorporated into α at residue 730, 731, or 413) may be used as indicators of the participation of a specific residue in a defined pathway for C_{439} oxidation in RNR (Figure 1). We have previously established that formation of $NH_2Y^\bullet$ is biphasic, giving rise to rate constants and amplitudes (as a percent of initial $Y_{122}^\bullet$) for $NH_2Y^\bullet$ formation of 19 s^{-1} (24%) and 2.7 s^{-1} (11%) at position 731 and 13 s^{-1} (20%) and 2.5 s^{-1} (19%) at position 730 (*15*). We have analyzed the kinetics of $NH_2Y^\bullet$ formation with all S:E pairs and argue that the slower rate constant is kinetically competent for deoxynucleotide formation (M. R. Seyedsayamdost, E. C. Minnihan, and J. Stubbe, unpublished results). An unexpected observation of our initial studies with the position 730- and 731-substituted proteins was the ability of these NH_2Y-α2s to catalyze deoxynucleotide formation, suggesting that $NH_2Y^\bullet$ at either position may be an intermediate on the pathway or may replace $Y_{122}^\bullet$ as a radical initiator.

In these studies, replacement of Y with the nonoxidizable F in the pathway at position 356 in β or position 731 in α, and incorporation of NH_2Y within the pathway after the block, resulted in no detectable $NH_2Y^\bullet$ by EPR analysis at 20 s or 2 min (Table 1). Since the EPR signal is always a composite of $Y^\bullet$ and $NH_2Y^\bullet$, a subtraction of the $Y^\bullet$ signal is required for spin quantitation of the two species. The broadness of the $Y^\bullet$ signal relative to the $NH_2Y^\bullet$ signal makes this subtraction straightforward, with the lower limit of detection of an $NH_2Y^\bullet$ estimated to be 3% of the total spin. It should be noted that cleaner subtractions are achieved when $Y_{122}^\bullet$ in an α:β complex is used as the reference, as the hyperfine interactions of $Y_{122}^\bullet$ in β appear to be subtly affected by formation of a complex with α.

To establish that $NH_2Y^\bullet$ is not generated transiently in the presence of a Y to F mutation, SF UV−vis spectroscopy was conducted and the reaction was monitored at 325 nm (320 nm) and 410 nm. An increase in the former absorption is associated with $NH_2Y^\bullet$ formation at position 730 (731) and a loss of the latter with $Y^\bullet$ loss. Monitoring a reaction at 325 nm is complicated by features of the diferric cluster that also absorb in this region. Thus, we have assumed transient features observed by SF are related to $NH_2Y^\bullet$ formation only if the rate constant and amplitude increase of the 325 nm feature parallels the rate constant and amplitude decrease of the 410 nm feature. As

indicated in Figure 2, in all experiments described herein in which the pathway has been "blocked", a small rise phase (approximately 2% of the $Y^{\bullet}$) has been observed at 325 nm. This rise is rapid (corresponding to a rate constant of $> 20\ s^{-1}$), has no corresponding decrease at 410 nm, and is attributed to a small change associated with the diferric $Y^{\bullet}$ cofactor. In our analysis, this feature is not considered further. Thus, the SF data are in agreement with the EPR results, indicating that a redox-active Y at positions 356 and 731 is a prerequisite for $NH_2Y^{\bullet}$ formation.

As noted above, at pH 7.0, NH_2Y is easier to oxidize than Y by 190 mV and thus could potentially be oxidized in an off-pathway process. To test this proposal, studies were conducted in which NH_2Y was incorporated in place of a residue proximal to the proposed pathway. Y_{413} (Figure 3) is located within 5 Å of both Y_{731} and Y_{730}, a distance feasible for a single oxidation "hop", and thus became the target of our off-pathway studies. Three experiments were conducted using mutants in which NH_2Y was site-specifically incorporated at position 413.

In the first, NH_2Y was incorporated at residue 413 while all other on-pathway residues were kept intact. In two additional experiments, a pathway block was introduced in the form of a Y to F mutation at either position 356 or 731. When the single mutant, $Y_{413}NH_2Y$-α2, was reacted with wt-β2, CDP, and ATP, SF experiments revealed formation of $NH_2Y_{413}^{\bullet}$ with a rate constant of $4-5\ s^{-1}$, corresponding to an 8% conversion of the initial $Y_{122}^{\bullet}$ to $NH_2Y_{413}^{\bullet}$ (Table 1). EPR analysis of the same reaction after 40 s was in agreement with the SF results, indicating the formation of a $NH_2Y^{\bullet}$ species accounting for 12% of the total spin (Figure 4A). The differences in the percent conversion of $Y_{122}^{\bullet}$ to $NH_2Y_{413}^{\bullet}$ as measured by SF and EPR may be indicative of the error inherent to the two methods in quantitation of low levels of radical species. Alternately, the differences may arise from the 10-fold difference in protein concentration used in the two experiments (*38*). As argued above, the rate constant and accumulation of $NH_2Y^{\bullet}$ are indicative of the relevance of that specific residue to catalysis in RNR. The rate constant of $4.2\ s^{-1}$ for $NH_2Y_{413}^{\bullet}$ formation is slower by a factor of 4 and the amplitude reduced by 75% relative to those of $NH_2Y^{\bullet}$ formation at position 731. This result suggests that NH_2Y at position 413 can be oxidized in an off-pathway fashion by either Y_{731} or Y_{356}. With F incorporated at position 731 and NH_2Y at position 413, $NH_2Y^{\bullet}$ is still observed. However, a fit of the SF data for the first 30 s gave a rate constant of $0.04\ s^{-1}$ and an amplitude of 12%. EPR spin quantitation of the same reaction after 40 s indicated 7% of the total spin was associated with the putative $NH_2Y^{\bullet}$ (Figure 4B). Finally, with F at position 356 and NH_2Y at position 413, no $NH_2Y^{\bullet}$ was detected (Figure 4C). Thus, the oxidation at position 413 appears to occur predominantly through Y_{356}. The very slow rate constant for $NH_2Y_{413}^{\bullet}$ formation with F at position 731 (~0.2% of that of $NH_2Y^{\bullet}$ formation at position 731 and ~2% of the steady-state rate constant for dCDP formation) and the complete absence of $NH_2Y_{413}^{\bullet}$ with F at position 356 suggest that radical formation at position 413 in the NH_2Y mutants results from off-pathway ET.

It is experimentally challenging to determine directly whether $NH_2Y_{413}^{\bullet}$ can participate as a chemically and kinetically competent intermediate in C_{439} oxidation. However, strong evidence that ET through residue 413 does not constitute a viable alternate radical pathway comes from the observation that no $NH_2Y^{\bullet}$ is generated in the reaction with $Y_{731}F/Y_{730}NH_2Y$-α2. Y_{413} cannot serve as a bypass to a block at residue 731 and thus cannot support the oxidation of Y at position 730 required for $C_{439}^{\bullet}$ formation and subsequent nucleotide reduction. The $NH_2Y_{413}^{\bullet}$ observed in experiments with $Y_{413}NH_2Y$-α2 or $Y_{731}F/Y_{413}$-NH_2Y-α2 thus results from an off-pathway oxidation and is nonfunctional.

Many examples of off-pathway oxidation exist in the literature for heme- and non-heme iron-dependent systems. Likewise, evidence for off-pathway oxidation has been reported previously in the class I *E. coli* RNR (*19*−*21*, *41*). The phenotypes usually are slow rate constants for radical formation and low amplitudes of new radical species. Thus, the experiments presented herein using F and NH_2Y as an oxidation block and trap, respectively, support the original proposal of Uhlin and Eklund for long-range oxidation of C_{439} in α via a conserved pathway of defined aromatic amino acids.

SUPPORTING INFORMATION AVAILABLE

EPR spectra and subtractions for reactions of $Y_{730}NH_2Y$-α2 and $Y_{731}NH_2Y$-α2 with $Y_{356}F$-β2 (Figure S1), SF traces for the reaction of $Y_{731}NH_2Y$-α2 with $Y_{356}F$-β2 (Figure S2), EPR spectrum and SF traces for the reaction of $Y_{731}F/Y_{730}NH_2$-Y-α2 with wt-β2 (Figure S3), SDS−PAGE of purified $Y_{413}NH_2Y$-α2 (Figure S4), plot of $Y_{730}F$-$\alpha2_{bound}$ versus $Y_{730}F$-$\alpha2_{free}$, used to extrapolate the K_d between wt-β2 and $Y_{413}NH_2Y$-α2 (Figure S5). This material is available free of charge via the Internet at http://pubs.acs.org.

REFERENCES

1. Gray, H. B., and Winkler, J. R. (2005) Long-range electron transfer. *Proc. Natl. Acad. Sci. U.S.A. 102*, 3534–3539.
2. Verkhovskaya, M. L., Belevich, N., Euro, L., Wikstrom, M., and Verkhovsky, M. I. (2008) Real-time electron transfer in respiratory complex I. *Proc. Natl. Acad. Sci. U.S.A. 105*, 3763–3767.
3. Igarashi, R. Y., and Seefeldt, L. C. (2003) Nitrogen fixation: The mechanism of the Mo-dependent nitrogenase. *Crit. Rev. Biochem. Mol. Biol. 38*, 351–384.
4. Loll, B., Kern, J., Saenger, W., Zouni, A., and Biesiadka, J. (2005) Towards complete cofactor arrangement in the 3.0 Å resolution structure of photosystem II. *Nature 438*, 1040–1044.
5. Page, C. C., Moser, C. C., Chen, X., and Dutton, P. L. (1999) Natural engineering principles of electron tunnelling in biological oxidation-reduction. *Nature 402*, 47–52.
6. Marcus, R. A., and Sutin, N. (1985) Nature of biological electron transfer. *Biochim. Biophys. Acta 811*, 265–322.
7. Langen, R., Chang, I. J., Germanas, J. P., Richards, J. H., Winkler, J. R., and Gray, H. B. (1995) Electron tunneling in proteins: Coupling through a β strand. *Science 268*, 1733–1735.
8. Osyczka, A., Moser, C. C., Daldal, F., and Dutton, P. L. (2004) Reversible redox energy coupling in electron transfer chains. *Nature 427*, 607–612.
9. Xiong, P., Nocek, J. M., Griffin, A. K., Wang, J., and Hoffman, B. M. (2009) Electrostatic redesign of the [myoglobin, cytochrome *b*5] interface to create a well-defined docked complex with rapid inter-protein electron transfer. *J. Am. Chem. Soc. 131*, 6938–6939.
10. Sjöberg, B. M., and Reichard, P. (1977) Nature of the free radical in ribonucleotide reductase from *Escherichia coli*. *J. Biol. Chem. 252*, 536–541.
11. Barry, B. A., and Babcock, G. T. (1987) Tyrosine radicals are involved in the photosynthetic oxygen-evolving system. *Proc. Natl. Acad. Sci. U.S.A. 84*, 7099–7103.
12. Stubbe, J., Nocera, D. G., Yee, C. S., and Chang, M. C. Y. (2003) Radical initiation in the class I ribonucleotide reductase: Long-range proton-coupled electron transfer? *Chem. Rev. 103*, 2167–2201.
13. Stubbe, J., and van der Donk, W. A. (1998) Protein radicals in enzyme catalysis. *Chem. Rev. 98*, 705–762.
14. Uhlin, U., and Eklund, H. (1994) Structure of ribonucleotide reductase protein R1. *Nature 370*, 533–539.
15. Seyedsayamdost, M. R., Xie, J., Chan, C. T., Schultz, P. G., and Stubbe, J. (2007) Site-specific insertion of 3-aminotyrosine into subunit α2 of *E. coli* ribonucleotide reductase: Direct evidence for involvement of Y730 and Y731 in radical propagation. *J. Am. Chem. Soc. 129*, 15060–15071.

16. Shih, C., Museth, A. K., Abrahamsson, M., Blanco-Rodriguez, A. M., Di Bilio, A. J., Sudhamsu, J., Crane, B. R., Ronayne, K. L., Towrie, M., Vlcek, A.Jr., Richards, J. H., Winkler, J. R., and Gray, H. B. (2008) Tryptophan-accelerated electron flow through proteins. *Science 320*, 1760–1762.
17. Cordes, M., Kottgen, A., Jasper, C., Jacques, O., Boudebous, H., and Giese, B. (2008) Influence of amino acid side chains on long-distance electron transfer in peptides: Electron hopping via "stepping stones". *Angew. Chem., Int. Ed. 47*, 3461–3463.
18. Bhattacharjee, S., Deterding, L. J., Jiang, J., Bonini, M. G., Tomer, K. B., Ramirez, D. C., and Mason, R. P. (2007) Electron transfer between a tyrosyl radical and a cysteine residue in hemoproteins: Spin trapping analysis. *J. Am. Chem. Soc. 129*, 13493–13501.
19. Lendzian, F. (2005) Structure and interactions of amino acid radicals in class I ribonucleotide reductase studied by ENDOR and high-field EPR spectroscopy. *Biochim. Biophys. Acta 1707*, 67–90.
20. Sahlin, M., Lassmann, G., Pötsch, S., Slaby, A., Sjöberg, B. M., and Gräslund, A. (1994) Tryptophan radicals formed by iron/oxygen reaction with *Escherichia coli* ribonucleotide reductase protein R2 mutant Y122F. *J. Biol. Chem. 269*, 11699–11702.
21. Sahlin, M., Lassmann, G., Pötsch, S., Sjöberg, B. M., and Gräslund, A. (1995) Transient free radicals in iron/oxygen reconstitution of mutant protein R2 Y122F. Possible participants in electron transfer chains in ribonucleotide reductase. *J. Biol. Chem. 270*, 12361–12372.
22. Choudhury, K., Sundaramoorthy, M., Hickman, A., Yonetani, T., Woehl, E., Dunn, M. F., and Poulos, T. L. (1994) Role of the proximal ligand in peroxidase catalysis. Crystallographic, kinetic, and spectral studies of cytochrome *c* peroxidase proximal ligand mutants. *J. Biol. Chem. 269*, 20239–20249.
23. Karthein, R., Dietz, R., Nastainczyk, W., and Ruf, H. H. (1988) Higher oxidation states of prostaglandin H synthase. EPR study of a transient tyrosyl radical in the enzyme during the peroxidase reaction. *Eur. J. Biochem. 171*, 313–320.
24. Sancar, A. (2003) Structure and function of DNA photolyase and cryptochrome blue-light photoreceptors. *Chem. Rev. 103*, 2203–2237.
25. Aubert, C., Vos, M. H., Mathis, P., Eker, A. P., and Brettel, K. (2000) Intraprotein radical transfer during photoactivation of DNA photolyase. *Nature 405*, 586–590.
26. Byrdin, M., Eker, A. P., Vos, M. H., and Brettel, K. (2003) Dissection of the triple tryptophan electron transfer chain in *Escherichia coli* DNA photolyase: Trp382 is the primary donor in photoactivation. *Proc. Natl. Acad. Sci. U.S.A. 100*, 8676–8681.
27. Lukacs, A., Eker, A. P., Byrdin, M., Villette, S., Pan, J., Brettel, K., and Vos, M. H. (2006) Role of the middle residue in the triple tryptophan electron transfer chain of DNA photolyase: ultrafast spectroscopy of a Trp → Phe mutant. *J. Phys. Chem. B 110*, 15654–15658.
28. Lukacs, A., Eker, A. P., Byrdin, M., Brettel, K., and Vos, M. H. (2008) Electron hopping through the 15 Å triple tryptophan molecular wire in DNA photolyase occurs within 30 ps. *J. Am. Chem. Soc. 130*, 14394–14395.
29. Climent, I., Sjöberg, B. M., and Huang, C. Y. (1992) Site-directed mutagenesis and deletion of the carboxyl terminus of *Escherichia coli* ribonucleotide reductase protein R2. Effects on catalytic activity and subunit interaction. *Biochemistry 31*, 4801–4807.
30. Ekberg, M., Sahlin, M., Eriksson, M., and Sjöberg, B.-M. (1996) Two conserved tyrosine residues in protein R1 participate in an intermolecular electron transfer in ribonucleotide reductase. *J. Biol. Chem. 271*, 20655–20659.
31. Rova, U., Goodtzova, K., Ingemarson, R., Behravan, G., Gräslund, A., and Thelander, L. (1995) Evidence by site-directed mutagenesis supports long-range electron transfer in mouse ribonucleotide reductase. *Biochemistry 34*, 4267–4275.
32. Rova, U., Adrait, A., Pötsch, S., Gräslund, A., and Thelander, L. (1999) Evidence by mutagenesis that Tyr(370) of the mouse ribonucleotide reductase R2 protein is the connecting link in the intersubunit radical transfer pathway. *J. Biol. Chem. 274*, 23746–23751.
33. Seyedsayamdost, M. R., Yee, C. S., Reece, S. Y., Nocera, D. G., and Stubbe, J. (2006) pH rate profiles of F_nY_{356}-R2s (n = 2, 3, 4) in *Escherichia coli* ribonucleotide reductase: Evidence that Y_{356} is a redox-active amino acid along the radical propagation pathway. *J. Am. Chem. Soc. 128*, 1562–1568.
34. Seyedsayamdost, M. R., and Stubbe, J. (2006) Site-specific replacement of Y_{356} with 3,4-dihydroxyphenylalanine in the β2 subunit of *E. coli* ribonucleotide reductase. *J. Am. Chem. Soc. 128*, 2522–2523.
35. Seyedsayamdost, M. R., Chan, C. T., Mugnaini, V., Stubbe, J., and Bennati, M. (2007) PELDOR spectroscopy with DOPA-β2 and NH_2Y-α2s: Distance measurements between residues involved in the radical propagation pathway of *E. coli* ribonucleotide reductase. *J. Am. Chem. Soc. 129*, 15748–15749.
36. Seyedsayamdost, M. R., and Stubbe, J. (2007) Forward and reverse electron transfer with the Y356DOPA-β2 heterodimer of *E. coli* ribonucleotide reductase. *J. Am. Chem. Soc. 129*, 2226–2227.
37. Seyedsayamdost, M. R. (2007) Investigation of the mechanism of radical propagation in *E. coli* ribonucleotide reductase by site-specific incorporation of unnatural amino acids. Ph.D. Thesis, Massachusetts Institute of Technology, Cambridge, MA.
38. Ge, J., Yu, G., Ator, M. A., and Stubbe, J. (2003) Pre-steady-state and steady-state kinetic analysis of *E. coli* class I ribonucleotide reductase. *Biochemistry 42*, 10071–10083.
39. Reece, S. Y., Seyedsayamdost, M. R., Stubbe, J., and Nocera, D. G. (2007) Photoactive peptides for light-initiated tyrosyl radical generation and transport into ribonucleotide reductase. *J. Am. Chem. Soc. 129*, 8500–8509.
40. Reece, S. Y., Seyedsayamdost, M. R., Stubbe, J., and Nocera, D. G. (2007) Direct observation of a transient tyrosine radical competent for initiating turnover in a photochemical ribonucleotide reductase. *J. Am. Chem. Soc. 129*, 13828–13830.
41. Yee, C. S., Seyedsayamdost, M. R., Chang, M. C. Y., Nocera, D. G., and Stubbe, J. (2003) Generation of the R2 subunit of ribonucleotide reductase by intein chemistry: Insertion of 3-nitrotyrosine at residue 356 as a probe of the radical initiation process. *Biochemistry 42*, 14541–14552.
42. Climent, I., Sjöberg, B. M., and Huang, C. Y. (1991) Carboxyl-terminal peptides as probes for *Escherichia coli* ribonucleotide reductase subunit interaction: Kinetic analysis of inhibition studies. *Biochemistry 30*, 5164–5171.
43. Palmer, G. (1967) Electron paramagnetic resonance. *Methods Enzymol. 10*, 595–610.
44. Nordlund, P., Sjöberg, B. M., and Eklund, H. (1990) Three-dimensional structure of the free radical protein of ribonucleotide reductase. *Nature 345*, 593–598.